ACS APPLIED MATERIALS & INTERFACES

Research Article

www.acsami.org

Rapid and Highly Efficient Preconcentration of Eu(III) by Core–Shell Structured Fe_3O_4@Humic Acid Magnetic Nanoparticles

Shitong Yang,[†] Pengfei Zong,[†,‡] Xuemei Ren,[†] Qi Wang,[†] and Xiangke Wang*,[†]

[†]Key Laboratory of Novel Thin Film Solar Cells, Institute of Plasma Physics, Chinese Academy of Sciences, P.O. Box 1126, 230031, Hefei, People's Republic of China

[‡]School of Nuclear Science and Technology, Xi'an Jiaotong University, 710049, Xi'an, People's Republic of China

Supporting Information

ABSTRACT: In this study, humic acid-coated Fe_3O_4 magnetic nanoparticles (Fe_3O_4@HA MNPs) were synthesized using a chemical coprecipitation method and characterized in detail. The XRD analysis results showed that HA coating did not change the phase of Fe_3O_4 cores. The TEM image suggested that Fe_3O_4@HA MNPs had nearly uniform size without the observation of aggregation. The Fe_3O_4@HA MNPs were stable in solution and could be easily separated from aqueous solution using a magnetic separation method. A batch technique was adopted to investigate the removal efficiency of Fe_3O_4@HA MNPs toward Eu(III) under various environmental conditions. The kinetic process of Eu(III) sorption on Fe_3O_4@HA MNPs reached equilibrium within <30 min. The fast sorption kinetics and high sorption amount were attributed to the plentiful surface sites provided by the surface-coated HA macromolecules. The Fe_3O_4@HA MNPs was able to remove ~99% of Eu(III) in aqueous solution at pH 8.5. Except for SO_4^{2-} anions, the coexisting electrolyte ions had no significant competition effects on the removal of Eu(III) by Fe_3O_4@HA MNPs. The obvious sorption–desorption hysteresis suggested that the removal of Eu(III) was dominated by inner-sphere surface complexation. The sorption isotherm agreed well with the Langmuir model, having a maximum sorption capacity of 6.95×10^{-5} mol g^{-1}. The leaching test showed that the Eu(III)-loaded Fe_3O_4@HA colloids were capable to maintain high thermodynamic stability for long aging times. The findings herein suggested that Fe_3O_4@HA MNPs could be potentially used as a highly effective material for the enrichment and preconcentration of radionuclide Eu(III) or other trivalent lanthanides/actinides in geological repositories or in nuclear waste management.

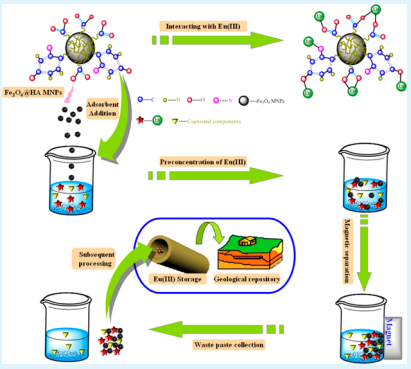

KEYWORDS: *Fe_3O_4@HA MNPs, Eu(III), material stability, sorption reversibility, magnetic separation, geological repository*

1. INTRODUCTION

With the development of nuclear energy and proceeding of various nuclear processes, a large amount of radioactive waste, such as ^{235}U, ^{235}Np, $^{152+154}Eu$, and ^{239}Pu, have been discharged into aquatic systems. The increasing level of toxic radionuclides exhibits a serious threat to human health, living resources, and ecological systems. For example, exposure to radioactive contaminants can cause serious diseases, such as diarrhea, vomiting, spasms, cardiovascular system damage, lymphatolysis, neurological disorder, leukemia, and even cancers. For the sake of ecological security and human health, the urgent issue is to develop advanced techniques and materials for the effective purification of radioactive wastewaters.

Recently, magnetic nanoparticles (MNPs) have been widely used in the environmental protection field, because of their extremely small size, absence of internal diffusion resistance, low cost, high surface-area-to-volume ratio, high magnetism, and high separation convenience.[1−4] However, bare MNPs are highly susceptible to air oxidation and are easily aggregated in various water systems,[5] which reduces their sorption capacity and accordingly restricts their large-scale application in environment remediation. To compensate for these two shortages, various natural and synthetic polymers have been introduced on MNP surfaces to synthesize novel adsorbents with high stability and super sorption capacity. Compared to naked MNPs and polymers, the obtained materials exhibited higher removal performance toward various heavy-metal ions and organic dyes.[6−10]

Humic substances (HS), including humic acid (HA), fulvic acids (FA), and humin, constitute ~60% of the dissolved organic carbon in aquatic systems.[11] The relatively strong binding of HS to metal oxides can significantly modify their physicochemical properties and sorption behaviors.[12,13] In addition, the strong complexation ability of HS toward heavy-metal ions and organic pollutants are important in regulating their mobility and transport in water systems. In view of this point, environmentalists introduced HA onto Fe_3O_4 MNP surfaces to prepare a novel Fe_3O_4@HA MNPs for the decontamination of polluted water systems. Liu et al. reported that the as-prepared Fe_3O_4@HA MNPs was stable in natural

Received: September 18, 2012
Accepted: November 26, 2012
Published: November 26, 2012

waters, tap water, and acidic/basic solutions ranging from 0.1 mol/L HCl to 2 mol/L NaOH with low leaching amounts of Fe and HA.[14] The Fe_3O_4@HA MNPs were able to remove ~99% of Hg(II) and Pb(II) and ~95% of Cd(II) and Cu(II) at optimized pH values. Besides, Fe_3O_4@HA MNPs were also proven to possess a fast sorption rate and high removal capacity toward organic dyes such as Methylene Blue and Rhodamin B.[15,16] More importantly, the dye-loaded Fe_3O_4@HA MNPs could be easily regenerated by eluting with acid solution. This advantage would greatly reduce the cost of sewage treatment. Niu et al. used Fe_3O_4@HA MNPs as a Fenton-like catalyst for the mineralization of sulfathiazole.[17] More than 95% of the sulfathiazole was degraded to ecofriendly inorganic ions or molecules (e.g., SO_4^{2-}, CO_2, and N_2) within a short reaction of 1 h. Based on the experimental results, they ascribed the high catalytic ability of Fe_3O_4@HA MNPs to the rapid regeneration of Fe(II) species and production of ·OH radicals. However, to the best of our knowledge, no study is focused on the application potential of Fe_3O_4@HA MNPs in radioactive wastewater disposal.

In this study, a core−shell-structured magnetic material was synthesized by decorating naked Fe_3O_4 MNPs with a HA coating. The physicochemical properties of naked Fe_3O_4 MNPs and as-prepared Fe_3O_4@HA MNPs were carefully characterized by Fourier transform infrared spectroscopy (FTIR), X-ray diffraction (XRD), zeta potential analysis, and magnetic measurements. In addition, the stability of the two materials was tested by measuring the leaching amounts of Fe and HA at different pH values. Afterward, the Fe_3O_4@HA MNPs were used for the removal of radionuclide Eu(III) from aqueous solutions. Herein, Eu(III) is selected as the target pollutant since its physicochemical behavior is similar to other trivalent lanthanides and actinides.[18,19] The overall performance of Fe_3O_4@HA MNPs was evaluated in terms of sorption kinetics, effects of various geochemical conditions, and leaching test. The application possibility of Fe_3O_4@HA MNPs for the enrichment and storage of radionuclide Eu(III) were further evaluated based on the experimental findings.

2. EXPERIMENTAL DETAILS

2.1. Materials and Reagents. The HA sample was extracted from the soil of Hua-Jia County (Gansu Province, China) and was characterized in detail in our previous studies.[20−22] Radiotracer $^{152+154}$Eu(III) was obtained from China Isotope Corporation with a radioactive purity of >99%. All of the chemicals were purchased from Sinopharm Chemical Reagent Co., Ltd. (Shanghai, China), had analytical purity, and were used directly without any further purification. Milli-Q water (Millipore, Bedford, MA, USA) was used to prepare all solutions.

2.2. Preparation of Naked Fe_3O_4 and Fe_3O_4@HA MNPs. The naked and HA-coated Fe_3O_4 MNPs were prepared with a chemical coprecipitation method, as described in previous literature.[14] First, 8.5 g of $FeSO_4·7H_2O$ and 12.3 g of $FeCl_3·6H_2O$ were dissolved in 200 mL of Milli-Q water and heated to 90 °C. Afterward, 30 mL of ammonium hydroxide (25%) solution and 100 mL of NaCl solution containing 1.0 g of HA were rapidly and sequentially added into the vessel. Finally, the mixture was continually stirred at 90 °C for 40 min and then cooled to room temperature. The black Fe_3O_4@HA precipitates were recovered by using an external magnet. Afterward, the collected wet pastes were rinsed several times with ethanol and Milli-Q water and then dried in a vacuum oven. The control sample of naked Fe_3O_4 MNPs was synthesized in a similar way without HA addition.

2.3. Characterization. The FTIR spectra of naked Fe_3O_4, HA, and Fe_3O_4@HA MNPs were recorded with a FTIR spectrometer (Perkin−Elmer Spectrum 100, USA) in the range of 4000−400 cm^{-1}, using KBr pellets. The spectral resolution was set to 1 cm^{-1}, and 150 scans were collected for each spectrum. The XRD patterns of naked and Fe_3O_4@HA MNPs were recorded on a MAC Science Co. Model M18XHF diffractometer, using Cu Kα radiation. The measurements were carried out in the 2θ range of 10°−70° with a scanning step length of 0.02°. The transmission electron microscopy (TEM) images were performed on a JEOL Model 2010 microscope to characterize the morphology and size distribution of naked Fe_3O_4 and Fe_3O_4@HA MNPs. The zeta potentials of naked Fe_3O_4 and Fe_3O_4@HA MNPs were measured with a Zetasizer Nano ZS Analyzer. The zero point charge (pH_{zpc}) was obtained by interpolating the data to zero zeta potential. The specific surface areas of naked Fe_3O_4 and Fe_3O_4@HA MNPs were measured using the N_2−BET method. The magnetic measurements were performed in a MPMS-XL SQUID magnetometer.

2.4. Material Stability Test. To test the stability of naked Fe_3O_4 and Fe_3O_4@HA MNPs, these two materials were exposed to different solutions with pH ranging from 2.0 to 11.0. After stirring for 24 h, the solid and liquid phases were separated with an external magnet. The total dissolved iron content in the supernatant was quantitatively measured by atomic absorption spectrometry (AAS). The concentration of dissolved organic carbon was measured with a Phoenix 8000 UV-persulfate TOC Analyzer.

2.5. Experimental Procedure. All the experiments were conducted in 10-mL polyethylene centrifuge tubes, using a batch technique under ambient conditions. Briefly, the suspensions of Fe_3O_4@HA MNPs and background electrolyte solution were pre-equilibrated for 24 h, and then Eu(III) stock solution including trace quantities of radiotracer $^{152+154}$Eu(III) was added to achieve the desired concentrations of individual components. The pH values were adjusted to desired values by adding negligible amounts of HCl or NaOH solutions. The centrifuge tubes were gently shaken on a rotating oscillator for 24 h to achieve sorption equilibrium. Afterward, the samples were exposed to an external magnet to separate solid and liquid phases. The $^{152+154}$Eu(III) concentration in the supernatant was analyzed by liquid scintillation counting (Packard 3100 TR/AB Liquid Scintillation analyzer, Perkin−Elmer) with an ULTIMA GOLD AB (Packard) Scintillation cocktail. Under the assumption that the added radiotracer $^{152+154}$Eu(III) dispersed evenly in the nonradioactive Eu(III) stock solution and both of them have similar sorption behaviors, the sorption percentage of Eu(III) on Fe_3O_4@HA MNPs was calculated from the initial activity of $^{152+154}$Eu(III) (A_{tot}) in initial solution and that of $^{152+154}$Eu(III) in the supernatant (A_L) (i.e., R (%) = $100 \times [1 - (A_L/A_{tot})]$). Detailed experimental procedures for each functional parameter are described in the Supporting Information.

3. RESULTS AND DISCUSSION

3.1. Characterization. Figure S1A in the Supporting Information shows the FTIR spectra of naked Fe_3O_4, Fe_3O_4@HA MNPs, and pure HA. For naked Fe_3O_4 (curve A) and Fe_3O_4@HA MNPs (curve B), the peak at 586 cm^{-1} corresponds to the characteristic stretching vibration of the Fe−O bond. All the characteristic bands of pure HA (curve C) are present in the spectrum of Fe_3O_4@HA MNPs (curve B),[15−17] indicating that HA has been successfully introduced on Fe_3O_4 surfaces. The similar XRD patterns of naked Fe_3O_4 and Fe_3O_4@HA MNPs (see Figure S1B in the Supporting Information) suggest that the decoration process with HA coating does not change the cubic phase of Fe_3O_4 cores.[23] The comparison between the TEM images of naked Fe_3O_4 and Fe_3O_4@HA MNPs (see Figures S1C and S1D in the Supporting Information) demonstrates that the HA coating significantly enhances the dispersion of Fe_3O_4@HA MNPs in solution. Detailed discussions on the characterization of naked Fe_3O_4 and Fe_3O_4@HA MNPs are described in the Supporting Information.

Zeta potential measurements indicate that the pH_{zpc} values of naked Fe_3O_4 and Fe_3O_4@HA MNPs are identified to be ~6.8

and ~2.5, respectively (see Figure 1A). This variation trend suggests that HA has been successfully grafted on Fe_3O_4

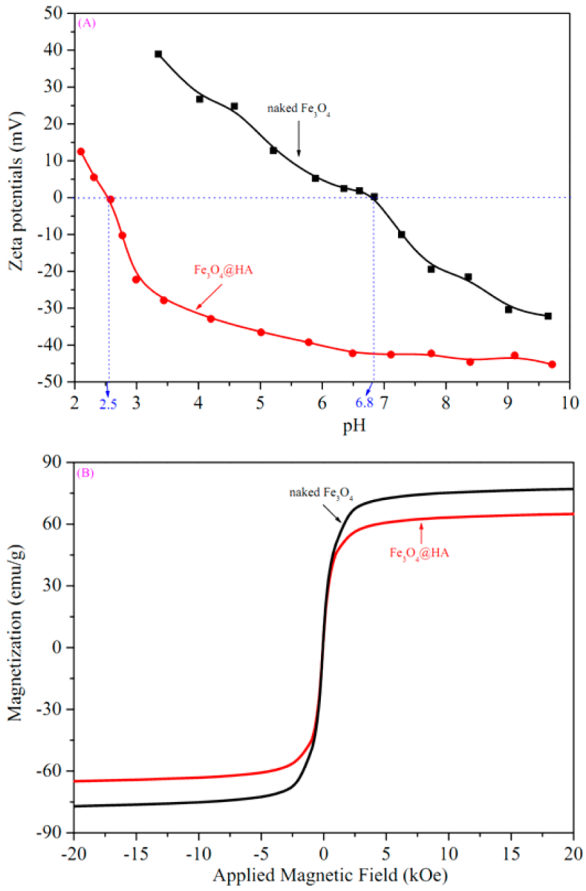

Figure 1. (A) Zeta potentials of naked Fe_3O_4 and Fe_3O_4@HA MNPs at various solution pH values. Conditions: T = 293 K, m/V = 0.5 g/L, I = 0.005 mol/L NaCl. (B) Magnetic hysteresis loops of naked Fe_3O_4 and Fe_3O_4@HA MNPs.

surfaces. The surface-coated HA will greatly influence the removal performance of Fe_3O_4@HA MNPs toward Eu(III) under various conditions. The specific surface areas of naked Fe_3O_4 and Fe_3O_4@HA MNPs are measured to be 63 and 61 m^2/g, respectively. Herein, the surface area of Fe_3O_4@HA MNPs is slightly lower than that reported in the previous literature (64 m^2/g),[14] which may be ascribed to the different HA origins. TOC measurement was conducted to quantify the HA content in Fe_3O_4@HA MNPs. The TOC contents for pristine HA and Fe_3O_4@HA MNPs are measured to be ~42.1% and ~6.53%, respectively. The HA content in Fe_3O_4@HA MNPs is then calculated to be ~15.5% (w/w). The magnetization curves have been previously used to quantitatively determine the grafted amount of natural organic matter on solid particles.[14] Herein, the saturation magnetization (M_s) of naked Fe_3O_4 and Fe_3O_4@HA MNPs are measured to be 77.1 and 64.9 emu/g, respectively (see Figure 1B). The difference of 12.2 emu/g indicates that the HA content in Fe_3O_4@HA MNPs is ~15.8% (w/w), which is compatible with that calculated from TOC measurement (~15.5% in w/w). The relatively high M_s value of Fe_3O_4@HA MNPs makes it easy to separate them from suspensions using a magnetic separation technique.

3.2. Material Stability. Figure 2 illustrates the leaching amounts of Fe from naked Fe_3O_4 and Fe_3O_4@HA MNPs as a

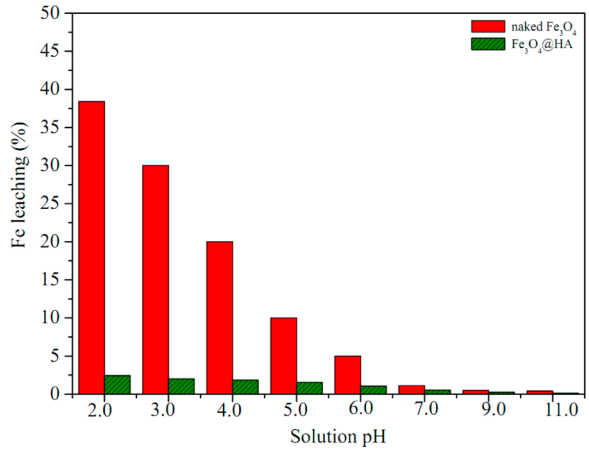

Figure 2. Relative proportion of Fe leaching from naked Fe_3O_4 and Fe_3O_4@HA MNPs at various solution pH values. Conditions: T = 293 K, m/V = 0.5 g/L, I = 0.005 mol/L NaCl.

function of solution pH values. For the two samples, the degree of Fe dissolution in acidic medium is higher than that in neutral and alkaline media. Specifically, the Fe leaching degree in the case of naked Fe_3O_4 is much higher than that of Fe_3O_4@HA MNPs under acidic conditions. At pH 2.0, the leaching percentage of Fe from naked Fe_3O_4 MNPs (38%) is almost 15-fold of that from Fe_3O_4@HA MNPs (2.5%). This phenomenon implies that the surface-coated HA layers protect the Fe_3O_4 cores from dissolution and, thus, significantly improve the stability of Fe_3O_4@HA MNPs under acidic conditions.[24−26] In addition, the leaching amount of HA from Fe_3O_4@HA MNPs is negligible. Herein, it is worth noting that the Fe_3O_4@HA MNPs are prepared using a chemical coprecipitation method under high alkaline conditions. The expanded HA morphology results in a tighter bond between HA functional groups and Fe_3O_4 surface sites, which reduces the leaching of Fe and HA from Fe_3O_4@HA MNPs. Previous literature implies that Fe_3O_4@HA MNPs are rather stable in tap water and natural waters without the dissolution of nanoparticle clusters.[14] The above-mentioned stability suggests that Fe_3O_4@HA MNPs can be used as suitable materials for the removal of Eu(III) from various water systems.

3.3. Effect of Contact Time. The kinetic data of Eu(III) sorption on naked Fe_3O_4 and Fe_3O_4@HA MNPs are shown in Figure 3A. It is clear that the removal percentages of Eu(III) in the two systems increase rapidly in the first 30 min of contact time, and then maintain level with increasing contact time. It is worth noting that the instantaneous time for solid−liquid separation, using an external magnet, can be neglected when testing the total contact time. For naked Fe_3O_4 MNPs, the fast Eu(III) removal rate arises from their nanoscaled particle size, which is beneficial for the transport of Eu(III) from bulk solution onto the surface binding sites.[27] For Fe_3O_4@HA MNPs, the rapid Eu(III) removal rate is attributed to the plentiful surface sites provided by the surface-coated HA. Davies et al.[28] proposed that HA macromolecular structure contains three forms of functional groups, i.e., site A (dicarboxylic acid groups on the rod exterior), site B (mixed ligands of catechol and amide groups), and site C (hollow interior including carbonyl and alcoholic groups). These three

dx.doi.org/10.1021/am3020372 | ACS Appl. Mater. Interfaces 2012, 4, 6891−6900

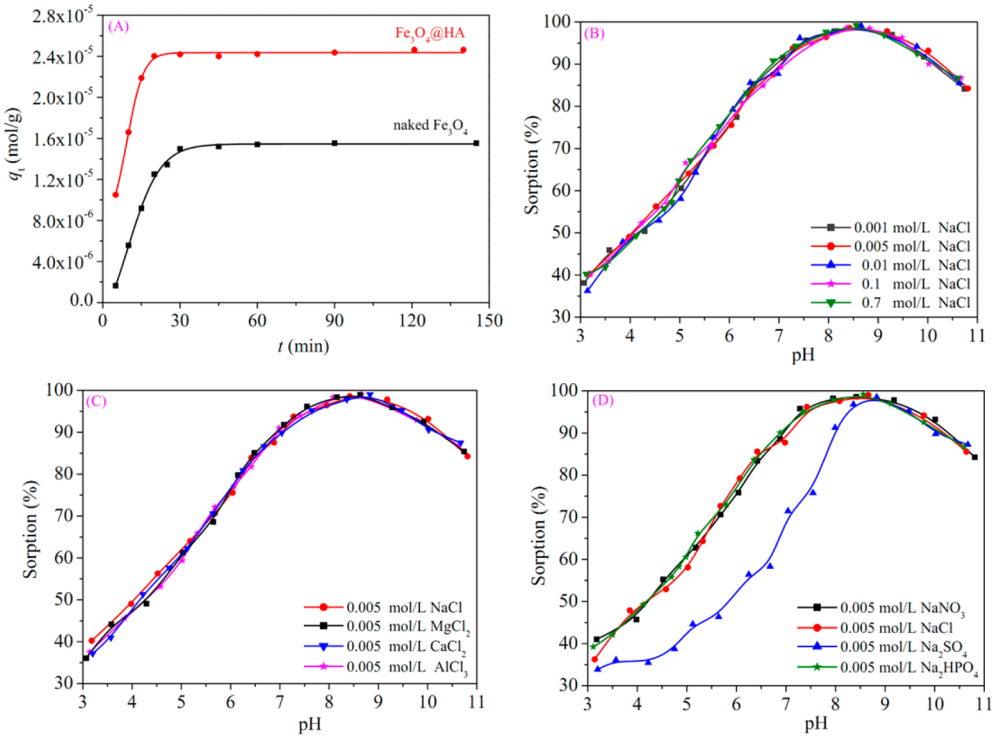

Figure 3. Sorption of Eu(III) on naked Fe_3O_4 and Fe_3O_4@HA MNPs under various environmental conditions. (A) Effect of aging time on Eu(III) sorption on naked Fe_3O_4 and Fe_3O_4@HA MNPs. Conditions: pH 5.0, T = 293 K, $C_{(Eu)initial}$ = 2.0 × 10^{-5} mol/L, m/V = 0.5 g/L, I = 0.005 mol/L NaCl. (B) Effect of pH and salinity on Eu(III) sorption on Fe_3O_4@HA MNPs. Conditions: T = 293 K, $C_{(Eu)initial}$ = 2.0 × 10^{-5} mol/L, m/V = 0.5 g/L. (C) Effect of coexisting cations on Eu(III) sorption on Fe_3O_4@HA MNPs. Conditions: T = 293 K, $C_{(Eu)initial}$ = 2.0 × 10^{-5} mol/L, m/V = 0.5 g/L. (D) Effect of coexisting anions on Eu(III) sorption on Fe_3O_4@HA MNPs. Conditions: T = 293 K, $C_{(Eu)initial}$ = 2.0 × 10^{-5} mol/L, m/V = 0.5 g/L.

categories of HA sites possess similar free binding energies, which means that the adsorbed Eu(III) encounters small kinetic barriers for transferring between different HA binding sites. Moreover, the absence of internal diffusion resistance may also contribute to the fast sorption rate. Equilibrium time is one of the important factors for evaluating the application potential of a synthetic material in sewage treatment. Herein, the short equilibrium time suggests that Fe_3O_4@HA MNPs can be potentially applied in continuous wastewater disposal. Based on the sorption kinetic data, a shaking time of 24 h was selected in the following experiments to ensure complete equilibrium.

The overall sorption rate and migration process of adsorbate at solid/water interfaces are controlled by the surface characteristics and diffusion resistance of solid particles. Therefore, the utilization of proper kinetic models can provide useful information for confirming the underlying mechanisms during the entire sorption process. In view of this point, the experimental kinetic data of Eu(III) sorption on naked Fe_3O_4 and Fe_3O_4@HA MNPs are simulated by the pseudo-first-order and pseudo-second-order models:[29,30]

pseudo-first-order model:

$$\ln(q_e - q_t) = \ln q_e - k_1 t$$

pseudo-second-order model:

$$\frac{t}{q_t} = \frac{1}{k_2 q_e^{\,2}} + \left(\frac{1}{q_e}\right) t$$

Herein, q_t and q_e represent the sorption amount of Eu(III) (in units of mol/g) at time t (min) and equilibrium time (min), respectively; k_1 (given in units of min^{-1}) and k_2 (expressed in units of g $(mol\ min)^{-1}$) are the kinetic rate constants of the pseudo-first-order and pseudo-second-order equations, respectively. The k_1 and $q_{e,cal}$ values of the pseudo-first-order model can be calculated from the linear plot of $\ln(q_e - q_t)$ vs t (figure not shown). The $q_{e,cal}$ and k_2 values of the pseudo-second-order model can be calculated from the linear plot of t/q_t vs t (see Figure S2 in the Supporting Information). The obtained kinetic parameters from both model fittings are listed in Table 1. The correlation coefficient (R^2) for the pseudo-second-order model is higher than that for the pseudo-first-order model. In addition, the $q_{e,cal}$ value obtained from the pseudo-second-order model fitting is more similar to the $q_{e,exp}$ value. These results shows that the pseudo-second-order model simulates the kinetic data better than the pseudo-first-order model. This phenomenon further indicates that the rate-controlling mechanism for Eu(III) sorption on naked Fe_3O_4

Table 1. Kinetic Parameters of Eu(III) Sorption on Naked Fe_3O_4 and Fe_3O_4@HA MNPs

correlation parameters	naked Fe_3O_4	Fe_3O_4@HA MNPs
pseudo-first-order model		
k_1 (min^{-1})	0.101	0.152
$q_{e,exp}$ (mol/g)	1.54 × 10^{-5}	2.46 × 10^{-5}
$q_{e,cal}$ (mol/g)	1.85 × 10^{-5}	2.61 × 10^{-5}
R^2	0.935	0.910
pseudo-second-order model		
k_2 (g/(mol·min))	1.06 × 10^4	1.29 × 10^4
$q_{e,exp}$ (mol/g)	1.54 × 10^{-5}	2.46 × 10^{-5}
$q_{e,cal}$ (mol/g)	1.60 × 10^{-5}	2.52 × 10^{-5}
R^2	0.998	0.999

dx.doi.org/10.1021/am3020372 | ACS Appl. Mater. Interfaces 2012, 4, 6891−6900

and Fe_3O_4@HA MNPs is chemisorption rather than mass transport.[31]

As shown in Figure 3A, the amount of Eu(III) adsorbed on Fe_3O_4@HA MNPs is much higher than that on naked Fe_3O_4 under the same experimental conditions. As mentioned above, the specific surface area of Fe_3O_4@HA MNPs (61 m^2/g) is comparable with that of naked Fe_3O_4 (63 m^2/g). This great proximity implies that specific surface area is not responsible for the different Eu(III) sorption amounts. Alternatively, the surface-linked HA is responsible for the higher sorption performance of Fe_3O_4@HA MNPs toward Eu(III). Previous laser particle size analysis showed that Fe_3O_4@HA MNPs possess smaller average value (140 nm) and narrower range of hydrodynamic size (104−189 nm) than those of naked Fe_3O_4 MNPs (250 nm, 160−366 nm).[14] This means that coating Fe_3O_4 MNPs with HA can efficiently reduce their aggregation in solution. The enhanced dispersion and stability of Fe_3O_4@HA MNPs by surface-linked HA can improve the availability of surface sites for binding Eu(III). HA has a macromolecular structure of aromatic and alkyl units attached with quinine, carboxyl, and phenolic hydroxyl sites. These binding sites have high capacity for complexation with Eu(III) and result in the formation of stable complexes. Besides, the aliphatic side chains and nitrogenous heterocycle in HA structure have unshared nitrogen electron pairs, which can primarily form coordination bonds with Eu(III) and partially contribute to Eu(III) removal.[32]

3.4. Effect of pH and Salinity. The pH-dependent sorption of Eu(III) on Fe_3O_4@HA MNPs was investigated at various electrolyte concentrations (i.e., 0.001, 0.005, 0.01, 0.1, and 0.7 mol/L NaCl solutions, respectively). This concentration range covers the salinity of fresh water and that of seawater. It is clear that solution pH plays an important role in Eu(III) sorption process. As shown in Figure 3B, the sorption of Eu(III) in 0.005 mol/L NaCl solution increases gradually from ∼40% to ∼99% as pH increases from 3.0 to 8.5, and slightly decreases from ∼99% to ∼85% in the pH range of 8.5−11.0. The occurrence of two inverse sorption trends suggests two different interaction mechanisms.

The observed Eu(III) sorption trends can be interpreted by the relative distribution of Eu(III) species in solution and the surface properties of Fe_3O_4@HA MNPs. Figure S3A in the Supporting Information illustrates the relative proportion of Eu(III) species computed by Visual MINTEQ ver. 3.0.[33] It is clear that Eu(III) in solution is predominated by positively charged species such as Eu^{3+}, $Eu(CO_3)^+$, $Eu(OH)^{2+}$, and $EuHCO_3^{2+}$ in the pH range of 3.0−8.5. As shown in Figure 2A, the pH_{zpc} value of Fe_3O_4@HA MNPs is ∼2.5. Hence, the Fe_3O_4@HA surfaces become negatively charged at pH >2.5. In addition, the successive deprotonation reaction of HA carboxylic and phenolic sites increases the surface electronegativity as the pH values increase. The increased attractive force between the negatively charged Fe_3O_4@HA surface sites and positively charged Eu(III) species enhances the formation of strong complexes. Moreover, the ionization of carboxylic sites increases the intermolecular repulsion in HA segment, resulting in the transformation of a highly coiled conformation at low pH values to an expanded network-like conformation at high pH values.[34] This variation trend will increase the contact area between Fe_3O_4@HA surface sites and Eu(III) species, which correspondingly enhances Eu(III) removal with increasing pH values. However, Eu(III) is mainly present as negatively charged $Eu(CO_3)_2^-$ species in solution at pH >8.5 (see Figure S3A in the Supporting Information). This species is difficult to be adsorbed on negatively charged Fe_3O_4@HA surfaces due to electrostatic repulsion, which accounts for the slight reducing of Eu(III) removal in this pH range. Besides, the slight decrease of Eu(III) removal may partially arise from the desorption of HA from Fe_3O_4@HA surfaces.[35] The freely dissolved HA can form complexes with Eu(III) species in solution and competitively inhibits the sorption of Eu(III) on Fe_3O_4@HA MNPs.

As shown in Figure 3B, the removal of Eu(III) is scarcely influenced by ionic strength variation over the entire pH range, suggesting that inner-sphere complexation is the dominant mechanism for Eu(III) immobilization on Fe_3O_4@HA MNPs.[36−38] In other words, the sorption procedure points to the formation of specific covalent bonds between Eu(III) and the electron-donating groups (i.e., various HA binding sites) on Fe_3O_4@HA surfaces. This phenomenon suggests that Fe_3O_4@HA MNPs are feasible for the decontamination of Eu(III)-bearing radioactive wastewater with various salinities (e.g., fresh water and seawater systems).

3.5. Effect of Coexisted Ions. Because of the heterogeneity and complexity of natural water and wastewater systems, the electrolyte cations therein may compete for the binding sites of solid particles (e.g., clays, metal oxides and natural organic matters). In addition, electrolyte anions always exhibit strong complexation ability toward both metal ions and solid surfaces. These two processes would greatly influence the migration and transformation of pollutants in environmental mediums. Based on these reasons, it is necessary to investigate the effect of coexisting ions on the purification of Eu(III)-bearing water systems.

Figures 3C and 3D shows the removal of Eu(III) by Fe_3O_4@HA MNPs, as affected by different electrolyte ions (viz, Na^+, Mg^{2+}, Ca^{2+}, Al^{3+}, NO_3^-, Cl^-, SO_4^{2-}, and PO_4^{3-}, respectively. The choice of the above-mentioned ions is based on their wide distribution in various water systems. The related experiments were conducted with chloride salts for cations and sodium salts for anions. Herein, the Eu(III) sorption in 0.005 mol/L NaCl solution was taken as a point of reference for quantitatively comparing the role of various ions. As can be seen from Figure 3C, the coexisting electrolyte cations have no significant competition effects on the removal of Eu(III) by Fe_3O_4@HA MNPs. The experimental results herein provide further evidence that the removal of Eu(III) is dominated by inner-sphere surface complexation rather than ion exchange/physical sorption. Generally, cations have a priority sequence for binding to organic matter as alkali-metal cations (e.g., Na^+ and K^+) < H^+ < alkaline-earth cations (e.g., Mg^{2+} and Ca^{2+}) < transitional monovalent cations (e.g., Ag^+) < transitional divalent cations (e.g., Co^{2+} and Ni^{2+}) < trivalent cations (e.g., Eu^{3+}).[39] Hence, alkali-metal and alkaline-earth cations are expected to exhibit little influence on the Eu(III) removal procedure. Specifically, it has been proved that monovalent and divalent cations (e.g., Na^+, Mg^{2+}, and Ca^{2+}) can lead to progressive HA aggregation and even precipitation by bridging with hydroxy and carboxyl sites on HA adjacent chains.[40] Besides, previous scanning electron microscopy (SEM) micrograph results suggested cation loading caused a conversion of HA fibrous morphology to a block-shaped morphology.[28] These two phenomena would partially reduce the number of Fe_3O_4@HA surface sites for binding Eu(III). However, our experimental result shows that the removal of Eu(III) is scarcely affected by the coexisting Na^+, Mg^{2+}, and Ca^{2+} cations.

The inconsistence herein suggests that the number of residual surface sites is abundant for binding Eu(III) species in solution. This deduction can be further supported by previous time-resolved laser-induced fluorescence spectroscopy analysis of HA-Eu(III) complexes, which suggests minor alteration of the Eu(III) chemical environment with increasing Ca^{2+} concentration.[41] The Al^{3+} cations in solution are reported to be preferentially attached on HA phenol-bearing sites.[42] In contrast, Eu(III) ions in solution are preferentially bound to HA carboxyl sites, as proved by C 1s-NEXAFS analysis and PHREEQC-Humic Ion Binding Model VI coupling.[43] Hence, the coexisting Al^{3+} cations in solution would not compete with Eu(III) for binding on Fe_3O_4@HA MNPs with regard to their affinity for disparate HA sites.

For coexisting electrolyte anions, NO_3^- and PO_4^{3-} have no obvious influence on Eu(III) removal over the entire pH range (see Figure 3D). In contrast, the coexisting SO_4^{2-} anions greatly reduce Eu(III) immobilization on Fe_3O_4@HA MNPs at pH <8.0, while no distinct influence is observed at higher pH values. Herein, the negatively charged NO_3^-, SO_4^{2-}, and PO_4^{3-} anions are incapable to be adsorbed on the negatively charged Fe_3O_4@HA surfaces, because of strong electrostatic repulsion. Instead, these three anions remain in solution and occur as counterions in the diffuse double layer.[44] As shown in Figure S3B in the Supporting Information, the coexistence of Eu(III) and NO_3^- species in solution results in the formation of soluble $Eu(NO_3)^{2+}$ species in the pH range of 3.0−7.0. However, the relative proportion of this species (~5%) is too small to influence the sorption of Eu(III) on Fe_3O_4@HA MNPs. Besides, no soluble Eu(III)−PO_4^{3-} complexes are expected to form when these two components are coexistent in solution (see Figure S3C in the Supporting Information). In view of this point, the inconspicuous effects of the PO_4^{3-} anion is attributed to the similarity between Eu(III) species in 0.005 mol/L NaH_2PO_4 solution (see Figure S3C in the Supporting Information) and that in 0.005 mol/L NaCl solution (see Figure S3A in the Supporting Information). In relative terms, the negative effect of SO_4^{2-} anions at pH <8.0 is an intricate situation and needs an intensive discussion. As shown in Figure S3D in the Supporting Information, Eu(III) in a SO_4^{2-}-containing system at pH <8.0 are present as Eu^{3+}, $EuSO_4^+$, $EuCO_3^+$, and $Eu(SO_4)_2^-$ species. More specifically, the relative proportion of Eu^{3+} species herein is much lower than that in SO_4^{2-}-free system (see Figure S3A in the Supporting Information). Instead, an additional $EuSO_4^+$ species with lower electropositivity becomes the predominant chemical form in solution. Compared with Eu^{3+} species, the $EuSO_4^+$ species exhibits lower affinity for negatively charged Fe_3O_4@HA surfaces. Besides, the interactions between Eu(III) and SO_4^{2-} species in solution lead to the formation of negatively charged $Eu(SO_4)_2^-$ species at pH <8.0 (see Figure S3D in the Supporting Information). This species is hardly adsorbed on negatively charged Fe_3O_4@HA surfaces, because of electrostatic repulsion, which diminishes the removal percentage of Eu(III) in this pH range. At pH >8.0, the dominant Eu(III) species in a SO_4^{2-}-containing system (Figure S3D in the Supporting Information) are similar to those in a SO_4^{2-}-free system (Figure S3A in the Supporting Information), which results in the similar Eu(III) removal trends in these two systems. The results herein indicate that the coexisting SO_4^{2-} exhibits significant influence on the migration and immobilization of Eu(III) in various water media under acidic and neutral conditions. In view of this point, the coexisting SO_4^{2-} anions in the system should be eliminated beforehand, to guarantee the removal efficiency of Fe_3O_4@HA MNPs toward Eu(III)-bearing wastewaters.

3.6. Effect of Solid Content and Temperature. Figure 4 shows the removal of Eu(III) by Fe_3O_4@HA MNPs at various solid contents and temperatures. It is clear that the sorption percentage is the highest at 313 K and is the lowest at 293 K (see Figure 4A), indicating that high temperature is beneficial for Eu(III) removal. Herein, the rise in temperature can enhance the Eu(III) activity in solution and accordingly strengthen their affinity to Fe_3O_4@HA surfaces.[45] Besides, higher temperature is expected to break some internal bonds and increase the number of available surface sites for binding Eu(III).[46] Moreover, the hydration sheath of Eu(III) ions can be effectively stripped at higher temperature, which facilitates the interactions between the dehydrated Eu(III) with Fe_3O_4@HA surface sites.

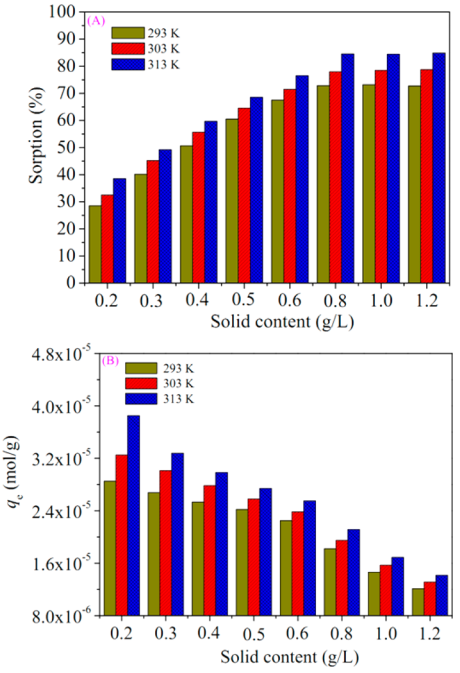

Figure 4. (A) Sorption percentage and (B) sorption amount of Eu(III) on Fe_3O_4@HA MNPs, as a function of solid content and temperature. Conditions: pH 5.0, $C_{(Eu(III))initial} = 2.0 \times 10^{-5}$ mol/L, I = 0.005 mol/L NaCl.

As can be seen from Figure 4A, the sorption percentage of Eu(III) at 293 K increases from ~28% to ~73% as the Fe_3O_4@HA dosage increases from 0.2 g/L to 0.8 g/L, and then its increase is negligible at Fe_3O_4@HA dosage higher than 0.8 g/L. The number of functional groups at Fe_3O_4@HA surfaces increases with increasing solid dosage. As a result, more binding sites are available to form complexes with Eu(III). However, the experimental results imply that the removal efficacy of Fe_3O_4@HA MNPs toward Eu(III) is not unboundedly in proportional to the solid dosage. From the aspect of reducing sewage disposal cost, one should choose appropriate Fe_3O_4@HA dosage based on the initial Eu(III) concentrations and related environmental criteria. Herein, the optimal dosage for Fe_3O_4@HA MNPs to decontaminate Eu(III) is 0.8 g/L. One can see from Figure 4B that the sorption amount of Eu(III) decreases gradually as the Fe_3O_4@HA dosage increases. Herein, the interactions between solid particles may cause the

desorption of some weak-linked Eu(III) ions from Fe_3O_4@HA surfaces. Besides, the decreased unsaturation of surface sites at higher solid dosage leads to the collision and overcrowding of Fe_3O_4@HA particles.[47] Furthermore, the increased aggregation probability of Fe_3O_4@HA particles at higher solid dosage may decrease the total surface area and prolong the diffusional path.[48] The above-mentioned phenomena would collectively lead to the reduction of Eu(III) sorption amount.

3.7. Sorption and Desorption Isotherms. The sorption and desorption experiments were carried out at pH 5.0 to further verify the binding mode and reversibility of Eu(III) sequestration on Fe_3O_4@HA MNPs. As shown in Figure 5, the

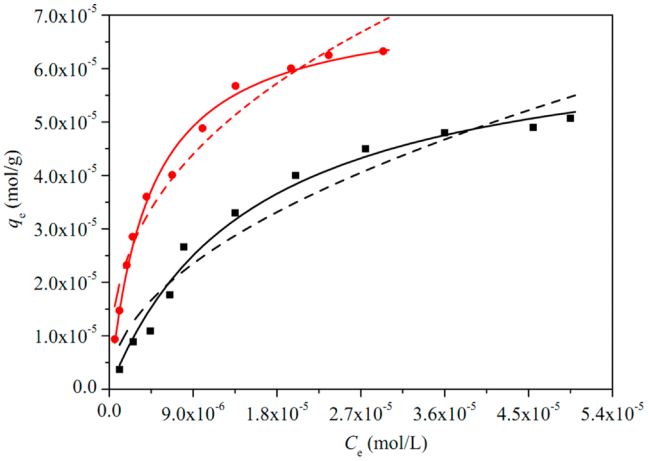

Figure 5. Sorption−desorption isotherms and Langmuir and Freundlich model fittings of Eu(III) on Fe_3O_4@HA MNPs. Conditions: pH 5.0, T = 293 K, m/V = 0.5 g/L, I = 0.005 mol/L NaCl. Symbols denote isotherms ((■) the sorption isotherm and (●) the desorption isotherm); solid lines represent the fitting curves of the Langmuir model, and dashed lines represent the fitting curves of the Freundlich model.

desorption isotherm is obviously higher than the sorption isotherm, which indicates that the sorption−desorption hysteresis occurs in the forward-sorption and backward-desorption processes. This phenomenon is indicative of an irreversible sorption, which further suggests that the immobilization of Eu(III) on Fe_3O_4@HA MNPs is dominated by strong chemical sorption (herein, inner-sphere complexation) rather than physical sorption.[49] Obviously, the formed complex is considered to be thermodynamic stable because of the formation of a tight bond. In view of this point, Fe_3O_4@HA MNPs can be potentially used as high-effective material for the enrichment and solidification of radionuclide Eu(III) from large volumes of wastewaters. The Eu(III)-loaded Fe_3O_4@HA MNPs can be easily separated from the solution via exposure to an external magnet. Afterward, the newly formed composite will be stored in specific containers for subsequent geological repository.

The sorption and desorption isotherms are simulated by the Langmuir and Freundlich equations (see Figure 5).

Langmuir equation:

$$q_e = \frac{bq_{max}C_e}{1 + bC_e}$$

Freundlich equation:

$$q_e = K_F C_e^{\,n}$$

Herein, C_e is the equilibrium concentration of Eu(III) that remained in solution (given in units of mol L^{-1}); q_e is the amount of Eu(III) adsorbed per weight unit of Fe_3O_4@HA MNPs after equilibrium (given in units of mol g^{-1}); q_{max} is the amount of Eu(III) at complete monolayer coverage (given in units of mol/g); b is a constant that relates to the sorption heat (given in units of L mol^{-1}); K_F is the sorption capacity when the Eu(III) equilibrium concentration is equal to 1 (mol^{1-n} L^n g^{-1}) and n represents the degree of sorption dependence at equilibrium concentration. The corresponding parameters calculated from the model fitting are listed in Table 2. One can see from the R^2 values that the Langmuir model simulates the sorption and desorption isotherms better than the Freundlich model. This phenomenon indicates that the binding energy on the entire surface of the Fe_3O_4@HA is uniform. In other words, the entire surface has identical sorption activity and therefore the immobilized Eu(III) ions do not interact or compete with each other, leading to the formation of a monolayer coverage on Fe_3O_4@HA surfaces. This phenomenon also manifests that chemisorption is the paramount removal mechanism.[50] Moreover, the as-prepared Fe_3O_4@HA MNPs have a finite specific surface and sorption capacity; thus, the sorption could be better described by the Langmuir model rather than by the Freundlich model, because an exponentially increasing sorption amount was assumed in the Freundlich model. The value of n calculated from the Freundlich model is from unity, indicating that a nonlinear sorption of Eu(III) takes place on Fe_3O_4@HA surfaces.

In order to verify the feasibility of using Fe_3O_4@HA MNPs as a potential sorbent for radioactive wastewater disposal, the maximum sorption capacity (i.e., q_{max} obtained from Langmuir model fitting) of Fe_3O_4@HA MNPs toward Eu(III) was carefully compared with those reported in previous literature.[38,51−56] Although a direct comparison of Fe_3O_4@HA MNPs with other sorbents is difficult due to the diversity between specific experimental conditions, it is clear that the maximum sorption capacity of Fe_3O_4@HA MNPs is higher than that of HA-MWCNT hybrids, 4-(2-pyridylazo) resorcinol-loaded polyurethane foam (PAR-loaded PUF), ZSM-5 zeolite, mesoporous Al_2O_3-intercalated expanded graphite (Al_2O_3/EG composite) and cellulose acetate (CA) membrane, comparable with 2-thenoyltrifluoroacetone-loaded polyurethane foam (HTTA-loaded PUR foam), while lower than that for an acrylamide-modified CA membrane (CA/AAM membrane) and graphene oxide (see Table 3). Herein, the higher sorption

Table 2. Parameters for Langmuir and Freundlich Models

	Langmuir			Freundlich		
condition	q_{max} (mol g^{-1})	b (L mol^{-1})	R^2	K_F (mol^{1-n} L^n g^{-1})	n	R^2
sorption	6.95×10^{-5}	6.51×10^{4}	0.991	7.44×10^{-3}	0.496	0.942
desorption	7.18×10^{-5}	2.35×10^{5}	0.993	3.64×10^{-3}	0.380	0.959

dx.doi.org/10.1021/am3020372 | ACS Appl. Mater. Interfaces 2012, 4, 6891−6900

Table 3. Comparison of Eu(III) Sorption Capacity of Fe_3O_4@HA MNPs with Other Sorbents

material	experimental conditions	q_{max} (mol g^{-1})	ref
HA-MWCNT hybrids	pH 4.5, T = 298 K	1.74×10^{-5}	51
PAR-loaded PUF	pH 7.0, T = 298 K	1.95×10^{-5}	52
ZSM-5 zeolite	pH 5.0, T = 298 K	2.16×10^{-5}	53
Al_2O_3/EG composite	pH 6.0, T = 293 K	3.34×10^{-5}	54
CA membrane	pH 5.0, T = 298 K	6.07×10^{-5}	55
Fe_3O_4@HA MNPs	pH 5.0, T = 293 K	6.95×10^{-5}	present study
HTTA-loaded PUR foam	pH 3.5, T = 293 K	8.20×10^{-5}	56
CA/AAM membrane	pH 5.0, T = 298 K	1.24×10^{-4}	55
graphene oxide	pH 4.5, T = 298 K	1.05×10^{-3}	38

capacity of CA/AAM membrane and graphene oxide may be partially attributed to the higher initial concentration range used in sorption isotherm experiments. However, these two materials are not able to support wide application, because of the complicated synthetic process, high raw-material cost, and high synthetic cost, as well as their potential ecological toxicity. In contrast, the core−shell-structured Fe_3O_4@HA MNPs can be easily synthesized by a simple chemical coprecipitation method. More importantly, Fe_3O_4@HA MNPs are low-cost and environmentally friendly since the main components (iron salts and HA) are abundant and harmless to ecosystems. In addition, Fe_3O_4@HA MNPs can be easily separated from aqueous solutions by using an external magnet. In view of the above reasons, Fe_3O_4@HA MNPs can be used as an attractive sorbent for the cost-effective purification of Eu(III)-bearing wastewater.

3.8. Regeneration and Reusability. From the standpoints of economic efficiency and environmental sustainability, it is essential to use renewable material, to minimize the wastewater treatment cost. In view of this point, the regeneration and reusability of Fe_3O_4@HA MNPs was tested to evaluate their application potential in the decontamination of Eu(III)-bearing wastewater. Since the sorption percentage of Eu(III) is lower at lower pH values, acid pickling is expected to be a feasible approach for the regeneration of Eu(III)-loaded Fe_3O_4@HA MNPs. Hence, 0.01 mol/L HCl solution was used to conduct regeneration operation and the regenerated Fe_3O_4@HA MNPs were used for six consecutive cycles. Considering the material loss during each cycle, the dosage of Fe_3O_4@HA MNPs and the volume of Eu(III) solution were adjusted to the comparable measurement. Figure 6 shows the relationship between regeneration cycle number and the corresponding Eu(III) sorption amount. One can see that the sorption amount of Eu(III) slightly decreases from 2.46×10^{-5} mol/g to 2.33×10^{-5} mol/g after six cycles. The puny decrease in sorption amount is attributed to the incomplete Eu(III) desorption from the surfaces of Fe_3O_4@HA MNPs. Overall, the excellent regeneration capacity and reusability suggest that Fe_3O_4@HA MNPs can support long-term use in sewage treatment with minimum replacement costs.

3.9. Eu(III) Leaching Test. The geological repository for high-level radioactive wastes is a complex system with successive barriers, mainly including the engineering barrier (e.g., nuclear waste pastes, storage containers, external package and backfill materials) and natural barrier (e.g., granite, clayrock, tuff, and etc.). With prolonged aging time, the groundwater around a geological repository gradually permeates the natural barrier and backfill materials, leading to fracture of the external package and even the internal containers. Besides, the heat released from radionuclide decay can increase the wall temperature of containers, thereby promoting their corrosion rate. In this case, the innermost nuclear waste pastes are expected to leak out and cause a serious threat to ecosystems as well as human health. In view of this point, it is necessary to test the thermodynamic stability of radionuclide-loaded materials, as affected by geochemical conditions.

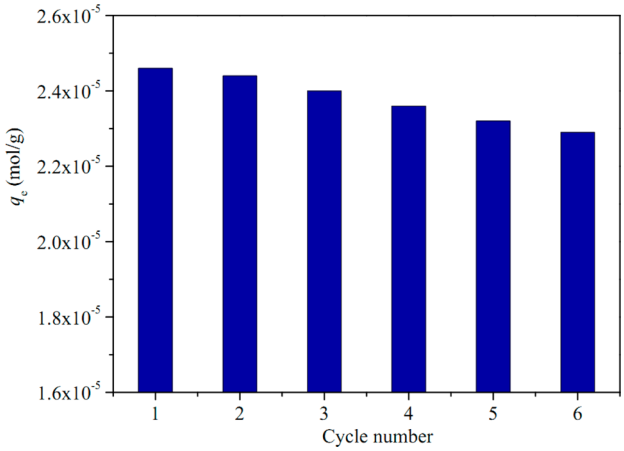

Figure 6. Recycling of Fe_3O_4@HA MNPs in the removal of Eu(III). Conditions: pH 5.0, T = 293 K, m/V = 0.5 g/L, I = 0.005 mol L^{-1} NaCl.

Herein, the effect of aging time on Eu(III) leaching from Eu(III)-loaded Fe_3O_4@HA colloids was investigated by resuspension tests. Briefly, the Fe_3O_4@HA MNPs laden with Eu(III) were resuspended in tap water, and the free Eu(III) concentration in supernatant was measured over various aging time (herein, from 1 to 90 d). Meanwhile, the leaching amounts of Fe and HA were also monitored by using AAS and a TOC analyzer. The results showed that the leaching of adsorbed Eu(III) was independent of aging time and the amount was negligible. In contrast, a slight increase of Fe leaching and a slight decrease of HA leaching were observed with prolonged aging time. Despite this, the leaching amounts could also be ignored for these two components, which are consistent with those reported in previous literature.[14,57] The results suggest that the Eu(III)-loaded Fe_3O_4@HA colloids are capable to maintain high thermodynamic stability for three months or even longer aging times. Considering the chronicity of Eu(III) migration in a real environment, a longer aging time is needed to precisely assess the thermodynamic stability of Eu(III)-loaded Fe_3O_4@HA colloids in a geological repository.

4. SIGNIFICANCE IN ENVIRONMENTAL REMEDIATION

This study reported the synthesis of core−shell-structured humic acid-coated Fe_3O_4 magnetic nanoparticles (Fe_3O_4@HA MNPs) by using a simple chemical coprecipitation method. The HA coating effectively improved the dispersion and stability of Fe_3O_4@HA MNPs in solution. Compared with naked Fe_3O_4 MNPs, the prepared Fe_3O_4@HA MNPs exhibited faster sorption kinetics and higher sorption amount toward Eu(III). In addition, Fe_3O_4@HA MNPs could be easily separated from aqueous solutions by using a magnetic separation technique at low magnetic field gradients. Moreover, the Eu(III)-loaded Fe_3O_4@HA MNPs exhibited satisfactory regeneration performance and reusability, which would be

expected to reduce the wastewater disposal expenses. The leaching test demonstrated that the Eu(III)-loaded Fe_3O_4@HA colloids could maintain high thermodynamic stability for three months. Considering the simple synthesis procedure, low cost, high removal efficiency, environmental friendliness, easy separation, and excellent stability, it is expected that Fe_3O_4@HA MNPs can be potentially used for the high-efficient preconcentration and solidification of Eu(III) or other trivalent lanthanides/actinides in geological repositories and nuclear waste management. Keeping in mind the heterogeneity and complexity of the real water environment, additional investigations are ongoing, to further verify the performances of Fe_3O_4@HA MNPs toward actual radioactive waste disposal.

■ ASSOCIATED CONTENT

Supporting Information

Detailed experimental procedures for each functional parameter, discussions on the characterization of naked Fe_3O_4 and Fe_3O_4@HA MNPs, kinetic model fitting and relative proportion of Eu(III) species in solution. This information is available free of charge via the Internet at http://pubs.acs.org.

■ AUTHOR INFORMATION

Corresponding Author

*Tel.: +86-551-5592788. Fax: +86-551-5591310. E-mail: xkwang@ipp.ac.cn.

Notes

The authors declare no competing financial interest.

■ ACKNOWLEDGMENTS

Financial support from National Basic Research Program of China (No. 2011CB933700) and National Natural Science Foundation of China (Nos. 41203086, 21077107, 21225730) is acknowledged.

■ REFERENCES

(1) Warner, C. L.; Addleman, R. S.; Cinson, A. D.; Droubay, T. C.; Engelhard, M. H.; Nash, M. A.; Yantasee, W.; Warner, M. G. *ChemSusChem* **2010**, *3*, 749−757.
(2) Ngomsik, A. F.; Bee, A.; Draye, M.; Cote, G.; Cabuil, V. *C. R. Chim.* **2005**, *8*, 963−970.
(3) Wang, P.; Lo, I. M. C. *Water Res.* **2009**, *43*, 3727−3734.
(4) Tuutijärvi, T.; Lu, J.; Sillanpää, M.; Chen, G. *J. Hazard. Mater.* **2009**, *166*, 1415−1420.
(5) Maity, D.; Agrawal, D. C. *J. Magn. Magn. Mater.* **2007**, *308*, 46−55.
(6) Mak, S. Y.; Chen, D. H. *Dyes Pigments* **2004**, *61*, 93−98.
(7) Banerjee, S. S.; Chen, D. H. *J. Hazard. Mater.* **2007**, *147*, 92−799.
(8) Zhou, L.; Gao, C.; Xu, W. J. *ACS Appl. Mater. Interfaces* **2010**, *2*, 1483−1491.
(9) Badruddoza, A. Z. M.; Tay, A. S. H.; Tan, P. Y.; Hidajat, K.; Uddin, M. S. *J. Hazard. Mater.* **2011**, *185*, 1177−1186.
(10) Yan, L.; Chang, P. R.; Zheng, P. Y.; Ma, X. F. *Carbohydr. Polym.* **2012**, *87*, 1919−1924.
(11) Antelo, J.; Arce, F.; Avena, M.; Fiol, S.; López, R.; Macías, F. *Geoderma* **2007**, *138*, 12−19.
(12) Ills, E.; Tombacz, E. *Colloid Surf. A* **2003**, *230*, 99−109.
(13) Ills, E.; Tombacz, E. *J. Colloid Interface Sci.* **2006**, *295*, 115−123.
(14) Liu, J. F.; Zhao, Z. S.; Jiang, G. B. *Environ. Sci. Technol.* **2008**, *42*, 6949−6954.
(15) Zhou, C. J.; Wu, Z.; Zhang, W. J.; Xia, M. X.; Dai, G. Z.; Zeng, G. M.; Zou, B. S.; Zhang, P. Y. *Funct. Mater. Lett.* **2011**, *4*, 373−376.
(16) Peng, L.; Qin, P. F.; Lei, M.; Zeng, Q. R.; Song, H. J.; Yang, J.; Shao, J. H.; Liao, B. H.; Gu, J. D. *J. Hazard. Mater.* **2012**, *209/210*, 193−198.
(17) Niu, H. Y.; Zhang, D.; Zhang, S. X.; Zhang, X. L.; Meng, Z. F.; Cai, Y. Q. *J. Hazard. Mater.* **2011**, *190*, 559−565.
(18) Tan, X. L.; Wang, X. K.; Geckeis, H.; Rabung, T. *Environ. Sci. Technol.* **2008**, *42*, 6532−6537.
(19) Bouby, M.; Geckeis, H.; Lützenkirchen, J.; Mihai, S.; Schäfer, T. *Geochim. Cosmochim. Acta* **2011**, *75*, 3866−3880.
(20) Fan, Q. H.; Tan, X. L.; Li, J. X.; Wang, X. K.; Wu, W. S.; Montavon, G. *Environ. Sci. Technol.* **2009**, *43*, 5776−5782.
(21) Yang, S. T.; Zhao, D. L.; Zhang, H.; Lu, S. S.; Chen, L.; Yu, X. J. *J. Hazard. Mater.* **2010**, *183*, 632−640.
(22) Yang, S. T.; Sheng, G. D.; Tan, X. L.; Hu, J.; Du, J. Z.; Montavon, G.; Wang, X. K. *Geochim. Cosmochim. Acta* **2011**, *75*, 6520−6534.
(23) Liao, M. H.; Chen, D. H. *J. Mater. Chem.* **2002**, *12*, 3654−3659.
(24) Matei, E.; Predescu, C.; Berbecaru, A.; Predescu, A.; Truşcă, R. *Dig. J. Nanomater. Biostruct.* **2011**, *6*, 1701−1708.
(25) Pang, Y.; Zeng, G. M.; Tang, L.; Zhang, Y.; Liu, Y. Y.; Lei, X. X.; Li, Z.; Zhang, J. C.; Liu, Z. F.; Xiong, Y. Q. *Chem. Eng. J.* **2011**, *175*, 222−227.
(26) Zhan, J. Y.; Tian, G. F.; Jiang, L. Z.; Wu, Z. P.; Wu, D. Z.; Yang, X. P.; Jin, R. G. *Thin Solid Films* **2008**, *516*, 6315−6320.
(27) Zhang, S.; Niu, H.; Cai, Y.; Zhao, X.; Shi, Y. *Chem. Eng. J.* **2010**, *158*, 599−607.
(28) Davies, G.; Fataftah, A.; Cherkasskiy, A.; Ghabbour, E. A.; Radwan, A.; Jansen, S. A.; Kolla, S.; Paciolla, M. D.; Sein, L. T.; Buermann, W.; Balasubramanian, M.; Budnicke, J.; Xing, B. *J. Chem. Soc., Dalton Trans.* **1997**, *21*, 4047−4060.
(29) Ho, Y. S.; Ofomaja, A. E. *J. Hazard. Mater.* **2006**, *129*, 137−142.
(30) Ho, Y. S.; McKay, G. *J. Environ. Sci. Health, A* **1999**, *34*, 1179−1204.
(31) Kamari, A.; Wan Ngah, W. S.; Chong, M. Y.; Cheah, M. L. *Desalination* **2009**, *249*, 1180−1189.
(32) Flaviane, V. K.; Leandro, V. A.; Laurent, G. F. *J. Hazard. Mater.* **2010**, *176*, 856−863.
(33) Gustafsson, J. P. Visual MINTEQ ver. 3.0. Department of Land and Water Resources Engineering, KTH (Royal Institute of Technology), SE-100 44, Stockholm, Sweden. Available at http://www2.lwr.kth.se/English/OurSoftware/vminteq/index.htm.
(34) Terashima, M.; Fukushima, M.; Tanaka, S. *Colloids Surf. A* **2004**, *247*, 77−83.
(35) Gu, B.; Schmitt, J.; Chen, Z.; Liang, L.; McCarthy, J. F. *Environ. Sci. Technol.* **1994**, *28*, 38−46.
(36) Rabung, T.; Stumpf, T.; Geckeis, H.; Klenze, R.; Kim, J. I. *Radiochim. Acta* **2000**, *88*, 711−716.
(37) Tan, X. L.; Fan, Q. H.; Wang, X. K.; Grambow, B. *Environ. Sci. Technol.* **2009**, *43*, 3115−3121.
(38) Sun, Y. B.; Wang, Q.; Chen, C. L.; Tan, X. L.; Wang, X. K. *Environ. Sci. Technol.* **2012**, *46*, 6020−6027.
(39) Zhao, D. L.; Chen, S. H.; Yang, S. B.; Yang, X.; Yang, S. T. *Chem. Eng. J.* **2011**, *166*, 1010−1016.
(40) von Wandruszka, R. *Geochem. Trans.* **2000**, *1*, 10−15.
(41) Marang, L.; Eidner, S.; Kumke, M. U.; Benedetti, M. F.; Reiller, P. E. *Chem. Geol.* **2009**, *264*, 154−161.
(42) Tang, J.; Johannesson, K. H. *Geochim. Cosmochim. Acta* **2003**, *67*, 2321−2339.
(43) Marsac, R.; Davranche, M.; Gruau, G.; Bouhnik-Le, C. M.; Dia, A. *Geochim. Cosmochim. Acta* **2011**, *75*, 5625−5637.
(44) Clare, R.; Collins, K.; Ragnarsdottir, V.; Sherman, D. M. *Geochim. Cosmochim. Acta* **1999**, *63*, 2989−3002.
(45) Partey, F.; Norman, D.; Ndur, S.; Nartey, R. *J. Colloid Interface Sci.* **2008**, *321*, 493−500.
(46) Genc-Fuhrman, H.; Tjell, J .C.; McConchie, D. *Environ. Sci. Technol.* **2004**, *38*, 2428−2434.
(47) Bhattacharyya, K. G.; Gupta, S. S. *Colloid Surf. A* **2008**, *317*, 71−79.
(48) Shukla, A.; Zhang, Y. H.; Dubey, P.; Margrave, J. L.; Shukla, S. S. *J. Hazard. Mater.* **2002**, *95*, 137−152.
(49) Zuo, L. M.; Yu, S. M.; Zhou, H.; Jiang, J.; Tian, X. *J. Radioanal. Nucl. Chem.* **2011**, *288*, 579−586.

(50) Zhou, Y. T.; Nie, H. L.; Branford-White, C.; He, Z. Y.; Zhu, L. M. *J. Colloid Interface Sci.* **2009**, *330*, 29−37.
(51) Fan, Q. H.; Shao, D. D.; Hu, J.; Chen, C. L.; Wu, W. S.; Wang, X. K. *Radiochim. Acta* **2009**, *97*, 1−8.
(52) Saeed, M. M.; Ahmed, M.; Chaudary, M. H.; Gaffar, A. *Solvent Extr. Ion Exch.* **2003**, *21*, 881−898.
(53) Shao, D. D.; Fan, Q. H.; Li, J. X.; Niu, Z. W.; Wu, W. S.; Chen, Y. X.; Wang, X. K. *Microporous Mesoporous Mater.* **2009**, *123*, 1−9.
(54) Sun, Y. B.; Chen, C. L.; Tan, X. L.; Shao, D. D.; Li, J. X.; Zhao, G. X.; Yang, S. B.; Wang, Q.; Wang, X. K. *Dalton Trans.* **2012**, *41*, 13388−13394.
(55) Zaki, A. A.; El-Zakla, T.; Abed El Geleel, M. *J. Membr. Sci.* **2012**, *401−402*, 1−12.
(56) Saeed, M. M. *J. Radioanal. Nucl. Chem.* **2003**, *256*, 73−80.
(57) Davis, A. P.; Bhatnagar, V. *Chemosphere* **1995**, *30*, 243−256.